

KECK/MOSFIRE SPECTROSCOPY OF $z = 7$ –8 GALAXIES: Ly α EMISSION FROM A GALAXY AT $z = 7.66$

MIMI SONG¹, STEVEN L. FINKELSTEIN¹, RACHAEL C. LIVERMORE¹, PETER L. CAPAK², MARK DICKINSON³, ADRIANO FONTANA⁴

Submitted to the ApJ

ABSTRACT

We report the results from some of the deepest Keck/MOSFIRE data yet obtained for candidate $z \gtrsim 7$ galaxies. Our data show one significant line detection with 6.5σ significance in our combined 10 hours of integration which is independently detected on more than one night, ruling out the possibility that the detection is spurious. The asymmetric line profile and non-detection in the optical bands strongly imply that the detected line is Ly α emission from a galaxy at $z(\text{Ly}\alpha) = 7.6637 \pm 0.0011$, making it the fourth spectroscopically confirmed galaxy at $z > 7.5$. This galaxy is bright in the rest-frame ultraviolet (UV; $M_{\text{UV}} \sim -21.2$) with a moderately blue UV slope ($\beta = -2.2^{+0.3}_{-0.2}$), and exhibits a rest-frame Ly α equivalent width of $\text{EW}(\text{Ly}\alpha) \sim 15.6^{+5.6}_{-3.6}$ Å. The non-detection of the 11 other $z \sim 7$ –8 galaxies in our long 10 hr integration, reaching a median 5σ sensitivity of 28 Å in the rest-frame $\text{EW}(\text{Ly}\alpha)$, implies a 1.3σ deviation from the null hypothesis of a non-evolving distribution in the rest-frame $\text{EW}(\text{Ly}\alpha)$ between $3 < z < 6$ and $z = 7$ –8. Our results are consistent with previous studies finding a decline in Ly α emission at $z > 6.5$, which may signal the evolving neutral fraction in the intergalactic medium at the end of the reionization epoch, although our weak evidence suggests the need for a larger statistical sample to allow for a more robust conclusion.

Subject headings: galaxies: evolution — galaxies: formation — galaxies: high-redshift

1. INTRODUCTION

The Ly α emission line is a unique tool as the line properties encode information about the scattering medium through which the photons have passed. During the past few years, in the present absence of a sensitive 21 cm signal from reionization, investigating the redshift evolution of the ‘Ly α fraction’, the fraction of Lyman-break galaxies (LBGs) which exhibit strong Ly α emission, has served as a valuable and feasible means of providing constraints on the ionization state of the intergalactic medium (IGM). Spectroscopic follow-up of LBGs has revealed that the Ly α fraction (typically defined as LBGs with rest-frame Ly α $\text{EW} > 25$ Å) steadily increases from $z = 3$ to $z = 6$, reaching $\sim 50\%$ for faint galaxies ($M_{\text{UV}} > -20.25$) at $z \sim 6$ (Stark et al. 2010, 2011). At higher redshifts of $z \sim 7$, however, initial expectations and attempts based on an extrapolation of the trend of the increasing Ly α fraction seen at lower redshifts found a reverse of the trend, showing only 20–30% of faint galaxies with Ly α emission (e.g., Fontana et al. 2010; Pentericci et al. 2011; Ono et al. 2012; Schenker et al. 2012; Finkelstein et al. 2013; Pentericci et al. 2014). This steep decrease beyond $z \sim 6$ is in line with measurements of Gunn-Peterson troughs (Gunn & Peterson 1965) in the spectra of distant quasars (Fan et al. 2006), which signal the (near) completion of reionization by $z \sim 6$.

Several attempts have been made to interpret the observed drop in the Ly α fraction in connection with the

neutral fraction of the IGM or different models of reionization. Earlier works suggested that, assuming that the observed drop in the Ly α fraction from $z \sim 6$ to $z \sim 7$ is entirely driven by the change in the IGM transmission, it requires a steep increase in the volume-averaged neutral fraction of $\Delta x_{\text{HI}} > 0.4$ –0.5 over $\Delta z = 1$ (Dijkstra et al. 2011; Pentericci et al. 2011). Alternatives have been subsequently proposed that account for the possibility of other sources of Ly α attenuation which alleviate the amount of the required increase in the neutral fraction. For example, Dijkstra et al. (2014) suggested that the change in the intrinsic physical properties of galaxies such as an increase in the escape fraction of ionizing photons can explain the observed drop with a mild increase in the neutral fraction of $\Delta x_{\text{HI}} = 0.1$ –0.2, and Bolton & Haehnelt (2013) argued that the rise of the neutral fraction of only $\Delta x_{\text{HI}} = 0.1$ by $z = 7$ is sufficient when accounting for self-shielding absorption systems (Lyman limit systems; LLSs) in the IGM which are expected to be abundant near the end of reionization (though see Mesinger et al. 2015). At $z \sim 7$, a sufficient sample has been assembled to start discerning between ‘patchy’ and ‘smooth’ models of Ly α attenuation. Pentericci et al. (2014) found from a compilation of observations at $z \sim 7$ that the ‘patchy’ model of Ly α attenuation (which does not necessarily literally mean a patchy reionization process but may instead signal the abundant LLSs; Mesinger et al. 2015), is favored over the ‘smooth’ attenuation model. These studies all highlight, although the interpretation is not straightforward, the potential of studying Ly α fraction as a valuable probe of reionization.

Because Ly α is redshifted into the near-infrared, the progress in identifying Ly α emission at a higher redshift of $z > 7$ had been relatively slow. However, the ad-

mmsong@astro.as.utexas.edu

¹ Department of Astronomy, The University of Texas at Austin, Austin, TX 78712, USA

² Spitzer Science Center, 314-6 Caltech, Pasadena, CA 91125, USA

³ National Optical Astronomy Observatory, Tucson, AZ 85719

⁴ INAF – Osservatorio Astronomico di Roma, via Frascati 33, 00040 Monteporzio, Italy

TABLE 1
SUMMARY OF $z_{\text{phot}} = 7\text{--}8$ CANDIDATES OBSERVED WITH MOSFIRE

ID ^a	R.A. (J2000)	Decl. (J2000)	J_{125}	H_{160}	M_{UV}	z_{phot}	z_{phot} 68% C.L. ^b	$p(z)_{Y\text{-band}}$ ^c	EW _{Lyα} ^d (Å)
z8_GSD_17938	3:32:49.94	−27:48:18.1	25.7	25.7	−21.6	8.07	[7.87, 8.37]	0.70	< 12
z7_GSD_10175	3:32:50.48	−27:46:56.0	25.7	25.6	−21.2	6.93	[6.14, 7.22]	0.37	< 15
z7_GSD_12816	3:32:44.89	−27:47:21.8	26.9	27.2	−20.2	6.81	[6.02, 7.20]	0.32	< 45
z7_MAIN_2852	3:32:42.56	−27:46:56.6	26.0	26.0	−20.9	6.85	[6.75, 6.93]	0.08	< 25
z7_MAIN_4005	3:32:39.55	−27:47:17.5	26.5	26.5	−20.7	7.55	[6.30, 7.55]	0.53	< 27
z7_MAIN_3474	3:32:38.80	−27:47:07.2	27.0	27.0	−20.0	7.41	[7.08, 7.54]	0.92	< 55
z8_GSD_2135	3:32:42.88	−27:45:04.3	26.9	26.8	−20.2	7.76	[1.84, 8.05]	0.49	< 39
z7_GSD_568	3:32:40.69	−27:44:16.7	26.9	26.8	−20.1	7.20	[6.62, 7.45]	0.62	< 35
z7_GSD_431	3:32:40.26	−27:44:09.9	26.6	26.7	−20.4	7.37	[6.66, 7.71]	0.70	< 28
z7_GSD_1273	3:32:36.00	−27:44:41.7	26.5	26.5	−20.4	6.86	[6.66, 7.05]	0.30	< 31
z7_GSD_3811	3:32:32.03	−27:45:37.1	25.8	25.9	−21.2	7.42	[6.71, 7.62]	0.73	< 15
z7_ERS_12098	3:32:35.44	−27:42:55.1	26.3	26.3	−20.7	7.17	[6.23, 7.25]	0.49	< 23

^a IDs from Finkelstein et al. (2015b).

^b 68% confidence level in photometric redshift.

^c Integral of $p(z)$ over the MOSFIRE Y -band spectral coverage.

^d Median 5σ rest-frame EW limit of Ly α (see Section 5).

vent of a new generation of ground-based near-infrared spectrographs with multiplexing capability and increased sensitivity has been changing the game by enabling more systematic searches for Ly α emission in $z \gtrsim 7$ galaxies. Yet, the current sample at $z > 7$ lacks statistical power to discern the two model of Ly α attenuation (e.g., Tilvi et al. 2014), as the required sample size is predicted to be at least several tens (Treu et al. 2012).

As expected, previous attempts in the search for Ly α emission at $z > 7$ have revealed that spectroscopically confirming galaxies at $z > 7$ via Ly α is challenging, yielding only 10 spectroscopically confirmed galaxies so far (Vanzella et al. 2011; Schenker et al. 2012; Ono et al. 2012; Shibuya et al. 2012; Finkelstein et al. 2013; Schenker et al. 2014; Oesch et al. 2015; Roberts-Borsani et al. 2015; Zitrin et al. 2015; see review in Finkelstein 2015a), and only four at $z > 7.5$, possibly due to an increased neutral fraction in the IGM. Despite these challenges, spectroscopic follow-up of galaxy candidates at these high redshifts, either yielding detections or non-detections, is valuable towards building up a statistical sample that is large enough to constrain the reionization process as well as studying in detail the physical properties of galaxies via further follow-up observations, and is thus being actively pursued.

This paper extends such previous and on-going attempts. In this study, we report Ly α emission from a galaxy at $z = 7.66$ in the Great Observatories Origins Deep Survey South (GOODS-S; Giavalisco et al. 2004) field. This is from a very deep spectroscopic follow-up campaign of $z \sim 7\text{--}8$ galaxy candidates with the Multi-Object Spectrometer For Infra-Red Exploration (MOSFIRE; McLean et al. 2012) on the Keck I 10 m telescope, where we push the median 5σ limiting sensitivity in line flux down to $\sim 5 \times 10^{-18}$ erg s $^{-1}$ cm $^{-2}$ between sky lines. Although limited by the small number of observed galaxies, we discuss the implications of our results in the context of the evolution of the Ly α visibility.

This paper is organized as follows. Section 2 describes our target selection, deep spectroscopic observations with MOSFIRE, and data reduction. Section 3 and 4 present the results from our spectroscopy and

our stellar population modeling, respectively. The implication of our observations on the Ly α visibility is presented in Section 5. The discussion and summary follow in Section 6. Throughout the paper, we adopt a concordance Λ CDM cosmology with $H_0 = 70$ km s $^{-1}$ Mpc $^{-1}$, $\Omega_M = 0.3$, and $\Omega_\Lambda = 0.7$. We use the AB magnitude system (Oke & Gunn 1983) and a Salpeter (1955) initial mass function (IMF) between 0.1 M_\odot and 100 M_\odot . We refer the *Hubble Space Telescope* (*HST*) bands F435W, F606W, F775W, F814W, F850LP, F098M, F105W, F125W, F140W, and F160W as B_{435} , V_{606} , i_{775} , I_{814} , z_{850} , Y_{098} , Y_{105} , J_{125} , JH_{140} , and H_{160} , respectively. All quoted uncertainties are 68% confidence intervals.

2. DATA

2.1. *HST* Data and Sample Selection

The targets were selected in the GOODS-S field from the parent sample from Finkelstein et al. (2015b). The parent sample was selected via photometric redshifts, which were estimated with EAZY (Brammer et al. 2008), using the *HST* dataset from the Cosmic Assembly Near-infrared Deep Extragalactic Legacy Survey (CANDELS; Grogin et al. 2011; Koekemoer et al. 2011) which incorporates all earlier imaging data over the field as described by Koekemoer et al. (2011, 2013). The MOSFIRE slit design was prepared using the MAGMA configurable slit unit (CSU) design tool. This tool takes as an input a list of objects, along with relative priorities. Our priority scheme was based on two quantities: the J_{125} -band magnitude of the source and the fraction of the source’s redshift probability distribution function (PDF; $p(z)$) which is encompassed by the MOSFIRE Y -band ($7.0 \lesssim z \lesssim 8.2$). We first assigned an initial priority based on the continuum magnitude, and then prioritized galaxies within that continuum magnitude bin by the normalized redshift integral. In this way, for two galaxies with similar redshift PDFs, the higher priority would go to the brighter one, while a faint galaxy with $z_{\text{phot}} \sim 7.5$ would be prioritized over a bright galaxy with $z_{\text{phot}} \sim 6.0$. In sum, we targeted 12 (8) galaxy candidates with $z_{\text{phot}} = 7\text{--}8$ (7.0–8.2). Of these, six galaxies have more than half of their redshift PDF placing Ly α in the MOS-

FIRE Y -band. The rest of slits in the mask were assigned to 18 galaxy candidates at lower redshifts of $z_{\text{phot}} = 4\text{--}6$ and one relatively bright star to monitor transparency and pointing accuracy. The median rest-frame absolute UV magnitude (M_{UV}) of our targets (assuming they are at their photometric redshifts) is -20.4 for the $z=7\text{--}8$ sample, ranging from -21.6 to -20.0 . The median H_{160} -band magnitude is 26.5 , ranging $[25.6\text{--}27.2]$. The full list of our $z = 7\text{--}8$ sample is tabulated in Table 1.

2.2. MOSFIRE Y -band Observation

Observations were taken with MOSFIRE on the Keck I telescope over 4 nights during January 11 and January 13–15, 2015. We used the Y -band filter, to search for $\text{Ly}\alpha$ emission at $7.0 < z < 8.2$, with a $0''.7$ slit width corresponding to a spectral resolution of $\sim 3 \text{ \AA}$ ($R = 3500$). Most of the data were taken with 180s exposures per frame, except that for the data taken on one night (January 15; for a total of 0.9 hr integration time) 60s exposures per frame were used. We adopted an ABBA dither pattern with an $\pm 1''.25$ offset along the slit for sky subtraction. The seeing measured from the star placed on a slit was in the range of $0.6\text{--}0.9''$, with a median/mean of $0.7''$. In total, we obtained a total on-source integration time of ~ 10 hr (from 2.8 hr (Jan 11) + 3.2 hr (Jan 13) + 3.2 hr (Jan 14) + 0.9 hr (Jan 15)), among which ~ 7.3 hr was obtained in good conditions. These observations are among the deepest observations ever taken for $z \gtrsim 7$ galaxies.

2.3. Data Reduction

Data reduction was performed with the public MOSFIRE data reduction pipeline (DRP; version 2015A), in which flat fielding, wavelength calibration, sky subtraction, and rectification were performed to create two-dimensional spectra with a spectral resolution of $1.09 \text{ \AA pixel}^{-1}$ and a spatial resolution of $0.18'' \text{ pixel}^{-1}$. Upon monitoring the centroid of the slit star in each raw frame, we identified a $\sim 1 \text{ pixel/hr}$ drift along the slit, which was also noted by several other studies (e.g., Kriek et al. 2015; Oesch et al. 2015). We thus split the data on each night into ~ 1 hr chunks and reduced them separately, to prevent loss of signal due to this drift.

Following this, analysis was done using our custom software. From the two-dimensional spectrum created by the pipeline, we combined the data from the four nights by generating final inverse-variance-weighted stacks for each object, following Gawiser et al. (2006). Spatial offsets between data chunks due to the drift were accounted for when combining data based on the centroids of the slit star. We extracted one-dimensional spectra at the expected position of each source with a width of $1.3''$ (about $1.8 \times$ the median Gaussian FWHM), using an optimal extraction algorithm described in Horne (1986). This extraction scheme is similar to inverse-variance weighting, but additional weight is given for each spatial pixel based on the expected spatial profile for each source (which is a Gaussian for our unresolved sources), reducing statistical noise in the extracted spectra compared to a simple boxcar extraction scheme.

Correcting for telluric absorption was done using the Kurucz (1993) model spectrum of the spectral type of the slit star (G5I). Absolute flux calibration was performed by comparing the WFC3 Y_{105} -band magnitude of

TABLE 2
SUMMARY OF Z7_GSD_3811

Emission Line Properties	
$F_{\text{Ly}\alpha}$ ($10^{-18} \text{ erg s}^{-1} \text{ cm}^{-2}$)	5.5 ± 0.9 (± 1.7)
Signal-to-noise Ratio	6.5
$\text{EW}_{\text{Ly}\alpha}$ (\AA) ^a	$15.6^{+5.9}_{-3.6}$ (± 4.7)
$z_{\text{Ly}\alpha}$	7.6637 ± 0.0011
σ_{blue} (\AA) ^b	$0.33^{+5.51}_{-0.32}$
σ_{red} (\AA) ^b	$6.49^{+0.32}_{-4.76}$
FWHM_{red} (\AA) ^c	15.0 ± 2.7
σ_{red} (km s^{-1}) ^d	180 ± 30
Physical Properties	
$\log M_*$ (M_{\odot})	$9.3^{+0.5}_{-0.4}$
UV slope β^e	$-2.2^{+0.3}_{-0.2}$
M_{UV}	$-21.22^{+0.06}_{-0.10}$
$E(B - V)$	$0.06^{+0.10}_{-0.04}$
$\text{SFR}_{\text{UV,obs}}$ ($M_{\odot} \text{ yr}^{-1}$)	19^{+2}_{-1}
$\text{SFR}_{\text{UV,corr}}$ ($M_{\odot} \text{ yr}^{-1}$) ^f	33^{+56}_{-9}

NOTE. — Listed in parentheses are systematic uncertainties.

^a Rest-frame equivalent width of $\text{Ly}\alpha$.

^b Observed line width of the blue and red side of the asymmetric Gaussian line profile, respectively.

^c Observed FWHM of the red side of the line.

^d Line-of-sight velocity dispersion inferred from the red side of the line. Corrected for instrumental resolution.

^e UV slope obtained in a same way as to Finkelstein et al. (2012), by fitting the wavelength window in the $1300\text{--}2600 \text{ \AA}$ region defined by Calzetti et al. (1994) of the best-fit SPS model as a power-law.

^f Dust-corrected SFR from the observed rest-frame UV magnitude and $E(B - V)$ obtained from the SPS model, assuming the Calzetti et al. (2000) extinction law and the Kennicutt (1998) conversion.

the slit star to the spectrum. This procedure accounts for the slit loss, assuming our targets are point sources unresolved under the seeing FWHM of our observations, which is a good approximation given that the small size of high redshift galaxies.

To check our flux calibration, we compared our calibration array with the total MOSFIRE Y -band throughput curve.⁵ We also utilised two bright continuum sources which were serendipitously included in our mask, to further verify our absolute flux calibration. Taking a similar approach to that of Kriek et al. (2015), we first convolved HST/Y_{105} images of the two sources and the slit star with a Gaussian kernel with width $\text{FWHM}_{\text{kernel}}^2 = \text{FWHM}_{\text{seeing}}^2 - \text{FWHM}_{H_{160}}^2$, to generate the Y -band image under the seeing of our spectroscopic observations. Then, we calculated the fraction of light of the two sources that are within our MOSFIRE slit layout. Comparing them to the fraction of light of the star within the slit (on which our absolute flux calibration is based), we calculated the expected flux ratio between our spectroscopic data and the broad-band flux (i.e., HST/Y_{105}) for the two sources due to the difference in the slit loss. This comparison shows that our absolute calibration (which affects our measurements of line flux and equivalent width, but not the significance

⁵ <http://www2.keck.hawaii.edu/inst/mosfire/throughput.html>

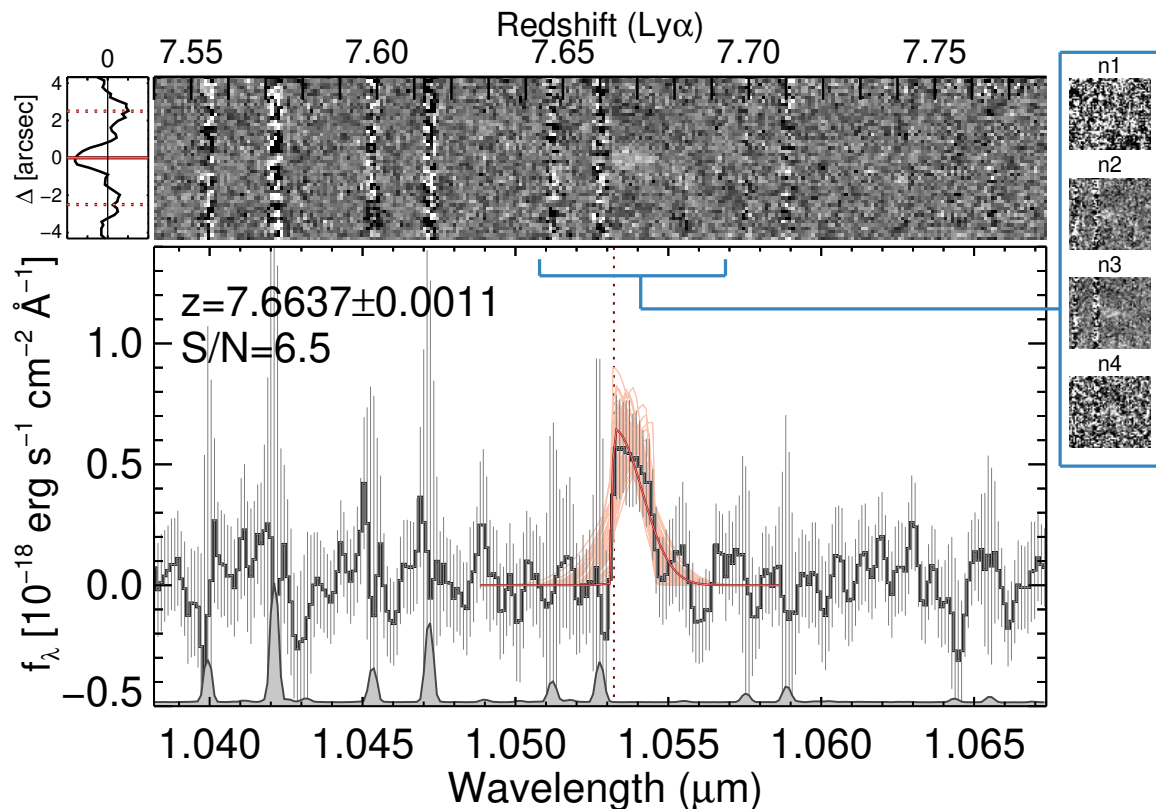


FIG. 1.— MOSFIRE Y -band 2D (*top*) and 1D (*bottom*) stacked spectra for the object with detected emission (z7_GSD_3811), showing a clear asymmetric line profile characteristic of Ly α emission. The displayed 1D spectrum was smoothed by the instrumental resolution (~ 3 Å). The best-fit asymmetric Gaussian curve and the line centroid are overplotted as the red thick solid curve and red dotted vertical line, respectively. The red thin curves are 100 Monte Carlo fits. The gray-shaded region near the bottom of the one-dimensional spectrum shows a scaled sky spectrum. Also shown on the upper-left corner is the 1D spectrum of the emission extracted along the spatial direction with inverse-variance weighting over the extraction width of the FWHM of the line. The red solid line and two red dotted lines overplotted are the expected spatial location of the positive peak and two negative peaks, respectively. We show in the blue box on the right side that the emission line is independently detected on all nights (n2, n3, n4) except in n1 which suffered from poor conditions, indicating that the chance of the detection being a spurious one is negligible.

of the detection) is accurate within 20–25%. We thus conservatively add a 30% systematic uncertainty in calibration in our error budget. The systematic uncertainties are indicated in Table 2, while the quoted uncertainties in the rest of the paper refer to random uncertainties.

Finally, to make sure that the error spectrum initially obtained from the pipeline does not underestimate the noise level, we scaled the error spectrum such that the standard deviation of the signal-to-noise ratio (SNR) in the sky dominated region is unity. The typical scale factor was 3.0 ± 0.1 .

3. RESULTS

3.1. Line Detection

We visually searched for emission lines in the extracted one-dimensional spectra as well as two-dimensional spectra at the expected positions of our targets. We take a conservative approach of presenting objects for which an emission line is independently detected on more than one night, minimizing the possibility of a spurious detection. In other words, we regarded it as a spurious detection if the emission was detected on only one night out of four nights. This criterion yielded only one line detection among the 30 objects originally targeted, at $\lambda_{\text{obs}} = 10532.2 \pm 1.3$ Å, and with 6.5σ significance. The rest remained undetected ($< 3\sigma$). Figure 1 shows

the one- and two-dimensional spectra of the object with emission, z7_GSD_3811. The emission is detected on more than one night at the same spatial and spectral location, with two negative peaks at the expected position from the adopted dithering pattern, ensuring that the line is real and not spurious.

Normally, we expect an asymmetric line profile with a sharp blue edge and gradually declining red tail for Ly α emission at high redshift due to absorption by neutral hydrogen in the interstellar and intergalactic medium. However, most of the proposed Ly α detections in other $z \gtrsim 7$ candidates have not shown highly significant evidence for asymmetry, possibly due to the low SNR for most of the detections. We find that our detected line displays an asymmetric line profile, making this object one of the first notable detections of asymmetry for a $z > 7$ Ly α line candidate. However, the significance is not strong due to the low SNR: the Gaussian line width on the blue and red side of the line is $0.33^{+5.51}_{-0.32}$ Å and $6.49^{+0.32}_{-4.76}$ Å, respectively. Due to the vicinity of a sky line located blueward of the line, the uncertainty in the line width on the blue side of the line (σ_{blue}) is large, yielding a weak constraint on the ratio between the line width on the red and blue side ($\sigma_{\text{red}}/\sigma_{\text{blue}} = 19.5^{+0.2}_{-19.3}$).

Assuming the line is Ly α , the implied redshift (based

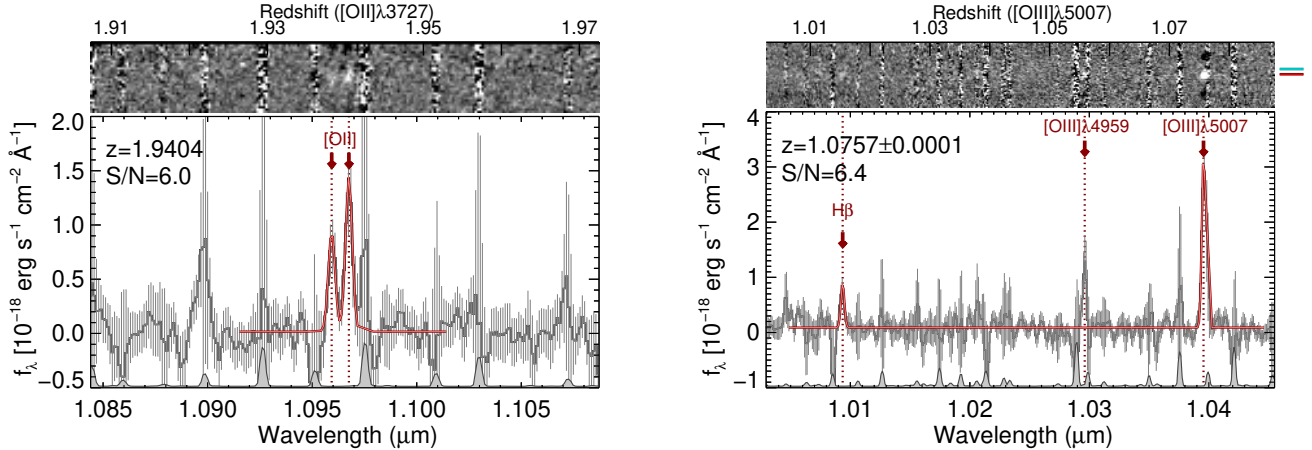


FIG. 2.— *Left*: an [O II] emitter serendipitously detected in the same mask under the same observing conditions as z7_GSD_3811. This source, detected at only slightly longer wavelength of $\lambda_{\text{obs}} = 1.096 \mu\text{m}$ than z7_GSD_3811, exhibits a well resolved doublet both in its 1D and 2D spectra, indicating the possibility of the line detected in z7_GSD_3811 being an unresolved [O II] doublet is low. *Right*: Detection of the H β and [O III] $\lambda\lambda 4959, 5007$ doublet from a source close to one of our original targets. The cyan and red lines on the right side of the 2D spectrum mark the expected positions of our original target and the nearby source, respectively. The position of the emission is spatially consistent with the position of the nearby source, not our original target.

on the line centroid defined as the wavelength of the peak of the Ly α emission) is $z(\text{Ly}\alpha) = 7.6637 \pm 0.0011$,⁶ placing it as presently the third most distant spectroscopically confirmed galaxy and the only galaxy at $z > 7$ in the GOODS-S field with a significant Ly α detection. The photometric redshift, estimated with EAZY (Brammer et al. 2008), is $z_{\text{phot}} = 7.42^{+0.20}_{-0.71}$, in good agreement with the spectroscopic redshift, as shown in the inset of Figure 3.

The line-of-sight velocity dispersion, derived from the Ly α line width on the red side of the line and corrected for instrumental resolution, is $180 \pm 30 \text{ km s}^{-1}$, similar to previously spectroscopically confirmed galaxies at similar redshifts (Oesch et al. 2015; Zitrin et al. 2015).

We fit an asymmetric Gaussian to the line to estimate the line flux of $(5.5 \pm 0.9) \times 10^{-18} \text{ erg s}^{-1} \text{ cm}^{-2}$. We estimated the rest-frame EW of Ly α emission from the observed Ly α flux and continuum flux density of the best-fit stellar population synthesis (SPS) model in a rest-frame 100 \AA box redward of the Ly α line (see Section 4). The inferred rest-frame EW of Ly α emission is modest with $15.6^{+5.9}_{-3.6} \text{ \AA}$, thus this object would not be classified as an Ly α emitter according to the traditional criterion of $\text{EW}(\text{Ly}\alpha) > 20 \text{ \AA}$. This value is also below the cutoff of $\text{EW}(\text{Ly}\alpha) > 25 \text{ \AA}$ (Stark et al. 2011) often adopted in the study of the evolution of the Ly α fraction at high redshift.

3.2. Low- z interpretations

We examined the possibility that the object is a foreground [O II] $\lambda\lambda 3726, 3729$, H β , [O III] $\lambda\lambda 4959, 5007$, or H α emitter. First, if the detected line is H β or one of the [O III] doublet, the other two lines would have been detected within our spectral coverage in regions free from

sky lines. We did not find any signal at the expected wavelengths of these lines.

Practically, the strong break observed between the z_{850} and Y_{105} bands (see Figure 3) rules out the possibility that the detected emission is H β , [O III], or H α , and leaves the only alternative possibility of the detected line being the [O II] doublet. If the detected emission line is an [O II] doublet at $z = 1.83$, the spectral resolution of MOSFIRE Y-band grating ($\sim 3 \text{ \AA}$) is sufficient to resolve the doublet. The possibility of the detected line being one of the two peaks, however, cannot be entirely ruled out. If the emission is the first peak of the [O II] doublet, we would have detected the second peak at $2-10\sigma$ significance at wavelengths clear of sky lines. On the other hand, if the emission is the second peak of the doublet, the centroid of the first peak would be behind the sky line located blueward of the detected line. To examine these possibilities, we performed simulations in which we inserted mock lines representing either the first or second peak of the [O II] doublet at the expected positions in the 2D spectrum. The spatial and spectral line profile of the mock line was assumed to be the same as that of the observed emission, and the flux was assigned based on the most unfavorable flux ratio that is physically allowed (i.e., the weakest line possible; $0.35 < f([\text{O II}]\lambda 3729)/f([\text{O II}]\lambda 3726) < 1.5$; Pradhan et al. 2006). Our simulation results indicate that due to its low flux and broad line profile, we would not be able to completely rule out the existence of the other line of the doublet based solely on our 2D spectrum. If the detected emission is indeed one of the [O II] doublet, the broad line width of the detected emission ($\text{FWHM} \sim 15 \text{ \AA}$) indicates that this galaxy hosts an active galactic nucleus (AGN).

As discussed above, it is unlikely that the detected line is an unresolved [O II] doublet given the spectral resolution. However, since the detected line has a moderate SNR of 6.5 σ , we conservatively leave this possibility open but further suggest evidence against it in Section 3.3 and 4.

⁶ Due to the IGM absorption and Ly α kinematics, the systemic redshift is likely to be slightly lower than the inferred redshift from the Ly α line. The systemic redshift (not corrected for IGM absorption) would be ~ 0.01 lower than the inferred redshift for the average velocity offsets of 200–400 km s^{-1} found in Lyman-alpha emitters and Lyman-break galaxies at lower redshift of $z \sim 2-3$ (e.g., Song et al. 2014; Steidel et al. 2010).

3.3. Serendipitous Line Detections at $z \sim 1-2$

In addition to the detected emission in z7_GSD_3811 from our targets, we identified two other emission lines in objects which serendipitously fell in slits.

The first object (R.A. = 3:32:43.22, Decl. = -27:47:12.9 (J2000)) shows an emission line with two peaks. Assuming that the detected line is an [O II] doublet, we derived its redshift to be $z = 1.94$. Its photometric redshift, $z_{\text{phot}} = 1.87^{+0.07}_{-0.08}$ (Dahlen et al. 2013), is in excellent agreement with the inferred [O II] redshift, thus we conclude that the detected line is the [O II] doublet. This [O II] doublet strengthens the possibility that the detected emission in z7_GSD_3811 is Ly α and not an unresolved [O II] doublet. The left panel of Figure 2 shows that the doublet in this object is spectrally well-resolved both in the 1D and 2D spectra, yet the observed wavelength and SNR are similar to those of z7_GSD_3811.

The second object (R.A. = 3:32:50.48, Decl. = -27:46:56.0 (J2000)) shows a prominent emission at $\lambda_{\text{obs}} = 10398 \text{ \AA}$, which we identified as an [O III] $\lambda 5007$ line (right panel of Figure 2). The other line of the doublet ([O III] $\lambda 4959$) is behind a sky line but still visible, and H β is detected at 5.6σ . Upon close inspection, we noted that the emission has an offset of 4–5 pixels along the spatial axis from our original target, which corresponds to $0.7\text{--}0.9''$. We identified a galaxy in proximity of our original target at this distance, thus we concluded that the emission is not from our target but from a foreground galaxy at $z = 1.08$.

4. STELLAR POPULATION MODELING & STACKING ANALYSIS

We performed a spectral energy distribution (SED) fitting analysis to the observed *HST*/ACS (B_{435} , V_{606} , i_{775} , I_{814} , z_{850}), *HST*/WFC3 (Y_{105} , J_{125} , H_{160}), and VLT/Haw-I K -band photometry of z7_GSD_3811, using the Bruzual & Charlot (2003) SPS models. Details on our modeling are described in Song et al. (2015). In addition to the *HST* bands originally included in the SED fitting in Song et al. (2015), in this work we included the K -band photometry from the Haw-I UDS and GOODS Survey (HUGS; Fontana et al. 2014) in the official CANDELS GOODS-S catalog (version 1.1). The *Spitzer*/IRAC photometry was excluded from the modeling, because z7_GSD_3811 is unfortunately heavily contaminated by a nearby bright source in IRAC. Thus, we do not have constraints on whether this galaxy exhibits the $4.5 \mu\text{m}$ color excess due to the strong [O III] line falling in the $4.5 \mu\text{m}$ band that some other studies have reported for spectroscopically-confirmed $z \sim 7\text{--}8$ galaxies (Finkelstein et al. 2013; Oesch et al. 2015; Zitrin et al. 2015; Roberts-Borsani et al. 2015).

As discussed in Section 3.2, the only alternative interpretation of the detected emission in z7_GSD_3811 is the [O II] doublet. Thus, we performed the SED fitting two times with a fixed redshift, first assuming the emission is Ly α , and then, assuming the emission is an [O II] doublet at $z([\text{O II}])=1.83$.

Figure 3 shows the model fit and stamp images. The results of our SED fitting analysis show that the high- z solution is preferred over the low- z solution, albeit mildly. For the high- z interpretation, because we did not fit bands shortwards of the Ly α line due to the large uncer-

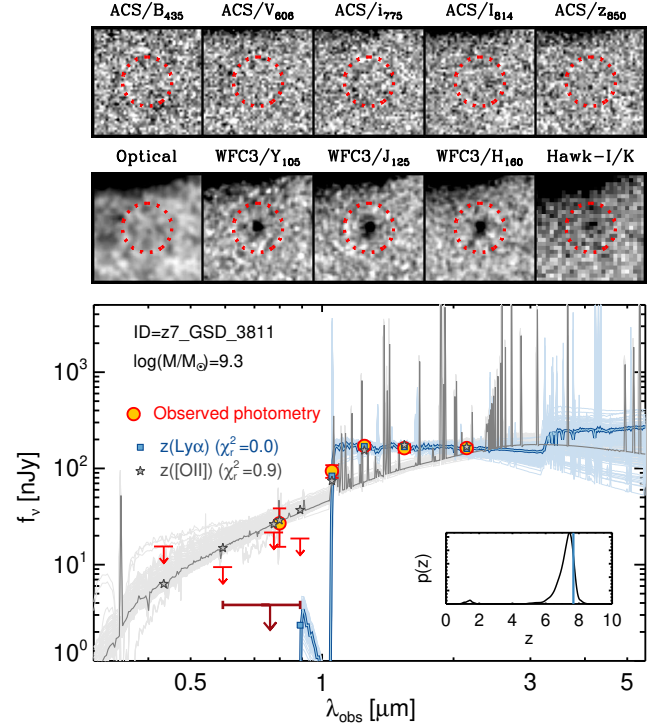


FIG. 3.— *Top*: postage stamp images of z7_GSD_3811 showing, from upper-left to lower-right, *HST*/ACS B_{435} , V_{606} , i_{775} , I_{814} , z_{850} , *HST*/ACS stack ($V_{606}+i_{775}+I_{814}+z_{850}$ bands), *HST*/WFC3 Y_{105} , J_{125} , H_{160} , and VLT/Haw-I K band. All stamp images are $3''$ on a side, north up, east to the left. *Bottom*: the observed SEDs (orange circles) and the best-fit SPS model and model bandpass-averaged fluxes (blue curve and blue squares) for z7_GSD_3811. For non-detections, we list 1σ upper limits (downward arrows).⁷ The dark red downward arrow represents the 1σ upper limit for the optical stack ($V_{606}+i_{775}+I_{814}+z_{850}$ bands). The best-fit SPS model and model fluxes under the alternative interpretation for the detected line (i.e., [O II] doublet at $z = 1.83$) are also shown as the gray curve and gray stars. The thin light-colored lines are 100 Monte Carlo fits, showing that the low- z solution is disfavored by the non-detection in the deep optical bands. The inset shows the probability distribution function of photometric redshift, in good agreement with the redshift of the Ly α emission (blue vertical line).

tainty in modeling the IGM attenuation, and because the source is highly contaminated by a nearby bright source in IRAC channels, only four bands (Y_{105} , J_{125} , H_{160} , and K) were used to constrain the fit, yielding $\chi_r^2 \sim 0$.

For the low- z interpretation, the non-detection in the deep optical bands⁷ and the strong break between z_{850} and Y_{105} of ~ 1.8 magnitude yield the only possible solution to be a dusty low-mass ($\log(M_*/M_\odot) = 9.1 \pm 0.1$) starburst galaxy with specific star-formation rate (sSFR) of $\log(\text{sSFR}/\text{yr}) = -7.1 \pm 0.2$. Yet, this low- z solution is disfavored over the high- z solution by non-detections in deep optical bands, with $\chi_r^2 \sim 0.9$.

To further probe the existence of any low level flux below the detection threshold of individual optical bands, we created a stack of V_{606} , i_{775} , I_{814} , and z_{850} band

⁷ Formally, our elliptical aperture photometry yields a 2.3σ detection in I_{814} band. However, the I_{814} band stamp image shows that all identifiable emissions are off-center and do not line up with near-infrared emission, indicating that they are likely background noise or from another unresolved faint source. Using a smaller, circular $0.4''$ diameter aperture centered on the near-infrared emission, we find no detection ($< 1\sigma$) in any optical band.

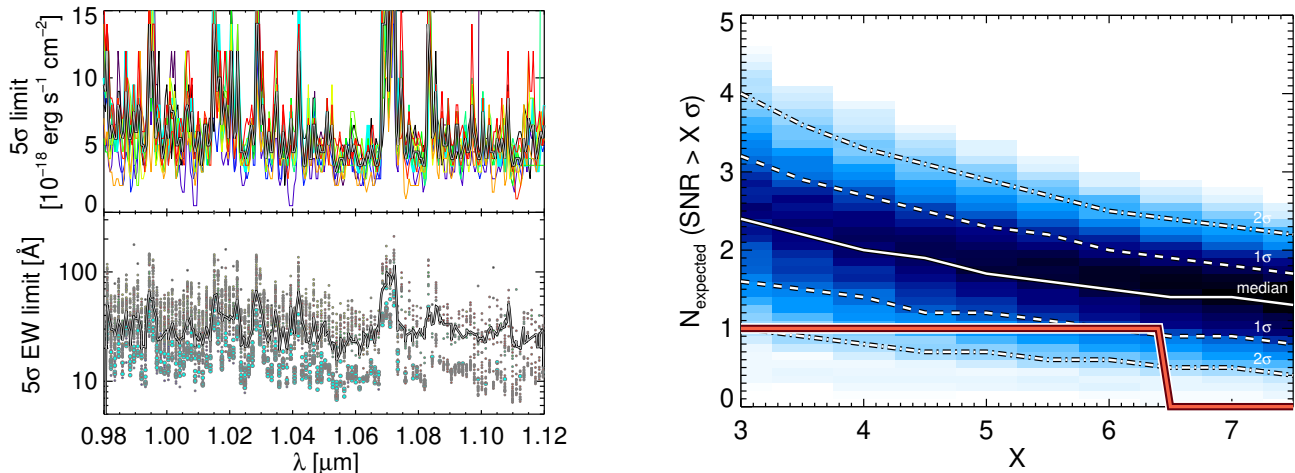


FIG. 4.— *Upper – left*: 5σ limiting line flux as a function of wavelength, estimated from a Monte Carlo simulation in which we inserted and recovered fake $\text{Ly}\alpha$ lines with varying line flux into our MOSFIRE spectra. The thin lines with different colors denote the estimates for each slit, and the black solid line indicates the median. *Bottom – left*: 5σ rest-frame $\text{EW}(\text{Ly}\alpha)$ limit as a function of wavelength. Each symbol denotes a trial of our Monte Carlo simulation, where different color indicates each object in our sample. The cyan circles represent the EW limits determined via Monte-Carlo trials for z7_GSD_3811. Our ~ 10 hr deep spectroscopy reaches a median rest-frame $\text{EW}(\text{Ly}\alpha)$ of 28 \AA between sky lines (range = $[12-55] \text{ \AA}$) for our $z = 7-8$ sample. *Right*: Probability distribution of the expected number of detections for the $\text{Ly}\alpha$ line (as a function of various detection thresholds X) for our MOSFIRE observations, assuming no evolution with redshift in the $\text{EW}(\text{Ly}\alpha)$ distribution from $3 < z < 6$. A darker blue color denotes higher probability. Our results of only one detection with 6.5σ (red line) is deviated from the null hypothesis of no EW evolution at 1.3σ (for $> 5\sigma$ detection, or 2σ if we push the detection significance down to $> 3\sigma$).

images. Prior to the stacking, the spatial resolution of the images were matched to that of the H_{160} -band and the units were converted to a physical unit. Then, the stack and stack rms map were generated by inverse-variance weighting, on which the stack flux and flux error were measured within a $0.4''$ diameter aperture using the Source Extractor package (Bertin & Arnouts 1996) and aperture-corrected using the ratio between the flux within a $0.4''$ aperture and total flux measured in the H_{160} band. We quantified the background noise as the Gaussian width of the flux distribution measured from 10^4 randomly placed apertures of the same size used in our original photometry in source-free regions of the stacked image. We checked that the flux error (3.8 nJy) measured from Source Extractor is slightly larger than the background noise (2.6 nJy), thus conservatively took the larger one. The stamp image and 1σ upper limit for the flux of the stack are shown in Figure 3. The stacking yielded no identifiable emission at the position of the source. The measured stack flux is 6σ lower than the prediction from the low- z solution, further indicating the preference for the high- z interpretation of the source.

We conclude that the detected line is $\text{Ly}\alpha$. z7_GSD_3811 is a galaxy bright in the UV with the rest-frame UV absolute magnitude of $M_{\text{UV}} \sim -21.2$, about two times brighter in luminosity than the characteristic UV magnitude of the rest-frame UV luminosity function at $z = 8$ of $M_{\text{UV}, z=8}^* = -20.48$ (Finkelstein 2015a). Other physical properties inferred from our SED fitting analysis indicate that z7_GSD_3811 is a typical galaxy at $z = 7-8$ for its UV magnitude, with a moderately blue UV slope ($\beta = -2.2^{+0.3}_{-0.2}$), dust-corrected UV-based SFR of $33^{+56}_{-9} M_{\odot}/\text{yr}$, and stellar mass of $\log(M_*/M_{\odot}) = 9.3^{+0.5}_{-0.4}$. Table 2 summarizes the physi-

cal properties of z7_GSD_3811.

5. $\text{Ly}\alpha$ VISIBILITY

Even with our deep integration of 10 hours, we detected only one $\text{Ly}\alpha$ emission line with a moderate rest-frame $\text{Ly}\alpha$ EW of 16 \AA . To put this result in context, we computed the number of detections expected from our observations, with the aim of placing constraints on the evolution of the $\text{Ly}\alpha$ visibility with redshift.

First, we quantified the limiting sensitivity of our observations by simulating $\text{Ly}\alpha$ lines in our MOSFIRE spectra. We modeled the $\text{Ly}\alpha$ line as an asymmetric Gaussian, similar to the detected line in z7_GSD_3811. Then, we inserted the lines with varying line fluxes into each of the actual 1D spectra in our mask at varying positions between the MOSFIRE Y-band wavelength coverage ($9800-11200 \text{ \AA}$), to find the line flux as a function of wavelength that ensures an X - σ detection ($X \geq 3$). The upper-left panel of Figure 4 presents the results, showing that our deep spectroscopy reaches a median 5σ limiting sensitivity in line flux of $\sim 5 \times 10^{-18} \text{ erg s}^{-1} \text{ cm}^{-2}$ between sky lines. Scaling our limiting sensitivity by \sqrt{t} , where t is the integration time, we find it consistent with the quoted limits of other MOSFIRE Y-band observations reported by Wirth et al. (2015).

For each object in our mask, we computed the X - σ limit in the rest-frame $\text{EW}(\text{Ly}\alpha)$ as a function of redshift (i.e., observed wavelength) for our observations. This was done via 1000 Monte Carlo realizations of the photometry for each object, for which we performed SED fitting. In each realization, the redshift was randomly drawn from the $p(z)$ distribution (thus the contaminant fraction, which is given by our $p(z)$, is accounted for in our results), and the corresponding continuum flux density redward of the $\text{Ly}\alpha$ was calculated from the best-

fit SPS model. The ratio of the limiting sensitivity, for which we take the median value at each wavelength as all the targets were observed in the same conditions in one MOSFIRE mask, to the continuum flux density in each realization gives the rest-frame $X\text{-}\sigma$ EW limit as a function of redshift (bottom-left panel of Figure 4).

By assuming an intrinsic rest-frame EW distribution for Ly α before being processed by the neutral gas in the IGM, we can compute how many sources are expected to be detected above our $X\text{-}\sigma$ EW limit. For the intrinsic rest-frame EW distribution for Ly α , $p(\text{EW}_{\text{intrinsic}})$, we adopted a log-normal form given by Schenker et al. (2014), which is based on the compilation of observations at $3 < z < 6$ when the universe is ionized. Then, $p(\text{EW}_{\text{intrinsic}})$ and our $X\text{-}\sigma$ EW limit inferred from our fake source simulation at the corresponding wavelength is compared, to estimate the probability that the line is detected. Here, we assumed that the $p(\text{EW}_{\text{intrinsic}})$ does not evolve as a function of redshift from $3 < z < 6$ to $z = 7\text{--}8$. Our analysis takes into account the effect of a sensitive wavelength dependency due to sky lines and the incomplete spectral coverage of the redshift probability distribution ($p(z)$), and is properly weighted by $p(z)$. The resulting probability distribution of the expected number of detections from our observations is shown in the right panel of Figure 4. Depending on the detection threshold adopted, our results show a 1–2 σ deviation from the null hypothesis of no evolution. For example, based on the Ly α EW distribution at lower redshift of $z \sim 3\text{--}6$ (assuming no evolution with redshift), we expect to detect $1.7^{+0.6}_{-0.5}$ ($2.4^{+0.8}_{-0.8}$) objects with $> 5\sigma$ (3σ) significance, for which our observations weakly reject at the 1.3 σ (2 σ) confidence level. Our results are conservative in the sense that had we assumed a zero low- z interloper fraction or used an extrapolation of the EW(Ly α) distribution from lower redshifts to $z \sim 7\text{--}8$, the inferred deviation from the expectation (and thus the implied decline in the Ly α fraction) would be higher.⁸

6. DISCUSSION AND SUMMARY

We have presented results from deep near-infrared Y-band spectroscopy targeting 12 galaxy candidates with $z_{\text{phot}} = 7\text{--}8$ in the GOODS-S field. Our long integration of ~ 10 hours with Keck/MOSFIRE enabled us to probe the Ly α emission down to a median 5σ rest-frame EW(Ly α) limit of 28 Å (ranging [12–55] Å; listed in Table 1). Despite our deep spectroscopy, we identified only one emission line at 6.5 σ significance, out of our 30 targets.

We claim that the detection is real, given that *i*) it was detected independently on more than one night, *ii*) at the expected spatial location, and *iii*) with two negative peaks at the positions expected from our dithering pattern.

This line is likely Ly α emission from a galaxy at $z = 7.6637$, based on *i*) its asymmetric line profile characteristic of Ly α at high redshift, *ii*) the non-

detection in the optical bands as well as an optical stack ($V_{606} + i_{775} + I_{814} + z_{850}$ bands), and *iii*) the inferred redshift in good agreement with its photometric redshift. While we cannot completely rule out the possibility that the detected line is an unresolved [O II] doublet from a galaxy at $z = 1.83$, we find it is unlikely, as a serendipitous [O II] emitter at $z \sim 1.9$ that falls in one of the slits, with the redshift difference of only $\Delta z \sim 0.1$ and with a similar SNR to that of $z7\text{-GSD_3811}$, shows clearly resolved double peaks both in our final stack and on individual nights.

The detected Ly α line has a modest rest-frame EW of 16 Å and a line flux of $(5.5 \pm 0.9) \times 10^{-18} \text{ erg s}^{-1} \text{ cm}^{-2}$. This galaxy is bright in the UV ($M_{\text{UV}} = -21.2$; $\sim 2L_{\text{UV}}^*$), and is a typical for its UV brightness in terms of UV slope ($\beta = -2.2$) and stellar mass ($\log(M_*/M_\odot) = 9.3$).

Identifying its nature via follow-up observations would be challenging but not impossible. Assuming this galaxy is an [O II] emitter at $z = 1.83$, other strong rest-frame optical emission lines (H β , [O III], and H α) all fall in between ground-based near-infrared bands, thus deep spaced-based grism may be the only possibility to detect those lines before the advent of the *James Webb Space Telescope*. If this galaxy is indeed at $z = 7.6637$ (with a normal stellar population), other emission features (e.g., C III] $\lambda\lambda 1907, 1909$) would be too weak to be detected in currently available data sets (e.g., *HST* grism) based on the typical flux ratio, unless Ly α is attenuated more than a factor of 15 by the IGM. However, this is unlikely given the Ly α EW distribution found by Stark et al. (2011) and Schenker et al. (2014) for its UV luminosity in galaxies at $3 < z < 6$. Additional integration in Y-band (for Ly α) or deep H-band observations (for C III]) can help verifying its identity. Alternatively, the Atacama Large Millimeter Array (ALMA) provides an opportunity to detect the [C II] line at 158 μm with less than an hour of integration, assuming that the empirical relation between SFR and [C II] 158 μm luminosity found for normal star-forming galaxies at high redshift (Capak et al. 2015) holds.

The rest of the targeted galaxies remain undetected, showing a 1.3 σ (2 σ) deviation from the expected number of detections (with $> 5\sigma$ ($> 3\sigma$) significance) when assuming no evolution in the Ly α EW distribution from lower redshifts of $3 < z < 6$ to $z = 7\text{--}8$. Our observations thus support the decline in the EW of Ly α at $z > 6.5$ of earlier studies (e.g., Schenker et al. 2014; Tilvi et al. 2014; Pentericci et al. 2014), which may be due to the increase of neutral gas in the IGM. However, the evidence from our observations alone is not conclusive due to the large statistical uncertainties. The addition of our sample to the compilation of previous data would be only incremental, thus we defer a detailed analysis on the evolution of the IGM neutrality to future studies with a larger statistical sample.

However, our results from very deep spectroscopy have implications for future observations. Recently, several studies (Roberts-Borsani et al. 2015; Zitrin et al. 2015) have claimed a high Ly α visibility in bright galaxies at $z > 7.5$ in the EGS field, which were selected based on red IRAC [3.6]–[4.5] colors indicative of strong [O III] emission. Combined with the recent discovery of Lyman

⁸ For reference, in a more traditional framework developed by Stark et al. (2010) of ‘Ly α fraction’, $z7\text{-GSD_3811}$ is not regarded as a Ly α -emitting galaxy, as the rest-frame EW is below the cutoff of 25 or 55 Å. Thus, the inferred Ly α fraction from our observation at $z \sim 7.5$ with EW > 25 or 55 Å is $X_{\text{Ly}\alpha} < 0.37$ for the UV-bright galaxies ($-21.75 < M_{\text{UV}} < -20.25$) and $X_{\text{Ly}\alpha} < 0.61$ for UV-faint galaxies ($-20.25 < M_{\text{UV}} < -18.75$; 1σ).

continuum leakers among strong [O III] emitters at low redshifts (Izotov et al. 2016; Vanzella et al. 2016) and the lack of significant Ly α detections in the GOODS-S field at comparable redshifts (before this study), this may signal the inhomogeneity of the reionization process on large scales. Indeed, while LAEs at lower redshifts of $3 < z < 6$ show that faint LAEs on average have a larger Ly α EW than bright ones (Stark et al. 2011), most spectroscopic campaigns at higher redshift targeting $z > 7$ galaxy candidates have only succeeded in detecting Ly α emission in bright galaxies (Finkelstein et al. 2013; Oesch et al. 2015; Zitrin et al. 2015; Roberts-Borsani et al. 2015). Our results are in line with these studies, yielding one Ly α detection from a bright ($L \sim 2L^*$) galaxy. However, it is noteworthy that our sole detection in z7_GSD_3811 is among those with the lowest EW limit (cyan circles in the bottom-left panel of Figure 4). This indicates that current spectroscopic campaigns at $z > 7$ are only reaching a sufficient depth for the brightest galaxies, leaving the possibility of detecting several galaxies in Ly α emission with modest Ly α EW in fainter galaxies open with deeper spectroscopy. Extremely deep spectroscopy (either by performing long

integrations on blank fields or by utilising magnification due to gravitational lensing) to better quantify the Ly α EW distribution, along with quantifying large scale spatial fluctuation in the reionization process from spatial clustering of Ly α emission from wide area surveys, will remain as a valuable probe of reionization in the near future.

MS acknowledges support from the NSF AAG award AST-1518183. MS and SLF acknowledge support from the NASA Astrophysics and Data Analysis Program award #NNX15AM02G issued by JPL/Caltech, as well as a NASA Keck PI Data Award, administered by the NASA Exoplanet Science Institute. This research is based on observations made with the Keck Telescope. The Observatory was made possible by the financial support of the W. M. Keck Foundation. We recognize and acknowledge the cultural role and reverence that the summit of Mauna Kea has within the indigenous Hawaiian community.

Facilities: Keck:I (MOSFIRE), *HST* (ACS, WFC3), VLT (HAWK-I)

REFERENCES

- Bertin, E., & Arnouts, S. 1996, *A&AS*, 117, 393
 Bolton, J. S., & Haehnelt, M. G. 2013, *MNRAS*, 429, 1695
 Brammer, G. B., van Dokkum, P. G., & Coppi, P. 2008, *ApJ*, 686, 1503
 Bruzual, G., & Charlot, S. 2003, *MNRAS*, 344, 1000
 Calzetti, D., Armus, L., Bohlin, R. C., et al. 2000, *ApJ*, 533, 682
 Calzetti, D., Kinney, A. L., & Storchi-Bergmann, T. 1994, *ApJ*, 429, 582
 Capak, P. L., Carilli, C., Jones, G., et al. 2015, *Nature*, 522, 455
 Dahlen, T., Mobasher, B., Faber, S. M., et al. 2013, *ApJ*, 775, 93
 Dijkstra, M., Wyithe, S., Haiman, Z., Mesinger, A., & Pentericci, L. 2014, *MNRAS*, 440, 3309
 Dijkstra, M., Mesinger, A., & Wyithe, J. S. B. 2011, *MNRAS*, 414, 2139
 Fan, X., Strauss, M. A., Becker, R. H., et al. 2006, *AJ*, 132, 117
 Finkelstein, S. L. 2015a, *arXiv:1511.05558*
 Finkelstein, S. L., Papovich, C., Dickinson, M., et al. 2013, *Nature*, 502, 524
 Finkelstein, S. L., Papovich, C., Salmon, B., et al. 2012, *ApJ*, 756, 164
 Finkelstein, S. L., Ryan, R. E., Jr., Papovich, C., et al. 2015b, *ApJ*, 810, 71
 Fontana, A., Dunlop, J. S., Paris, D., et al. 2014, *A&A*, 570, A11
 Fontana, A., Vanzella, E., Pentericci, L., et al. 2010, *ApJ*, 725, L205
 Gawiser, E., van Dokkum, P. G., Herrera, D., et al. 2006, *ApJS*, 162, 1
 Giavalisco, M., Ferguson, H. C., Koekemoer, A. M., et al. 2004, *ApJ*, 600, L93
 Grogin, N. A., Kocevski, D. D., Faber, S. M., et al. 2011, *ApJS*, 197, 35
 Gunn, J. E., & Peterson, B. A. 1965, *ApJ*, 142, 1633
 Horne, K. 1986, *PASP*, 98, 609
 Izotov, Y. I., Orlitová, I., Schaerer, D., et al. 2016, *Nature*, 529, 178
 Kennicutt, Jr., R. C. 1998, *ARA&A*, 36, 189
 Koekemoer, A. M., Anton, M., Faber, S. M., et al. 2011, *ApJS*, 197, 36
 Koekemoer, A. M., Ellis, R. S., McLure, R. J., et al. 2013, *ApJS*, 209, 3
 Kriek, M., Shapley, A. E., Reddy, N. A., et al. 2015, *ApJS*, 218, 15
 Kurucz, R. 1993, *ATLAS9 Stellar Atmosphere Programs and 2 km/s grid*. Kurucz CD-ROM No. 13. Cambridge, Mass.: Smithsonian Astrophysical Observatory, 1993., 13,
 McLean, I. S., Steidel, C. C., Epps, H. W., et al. 2012, *Proc. SPIE*, 8446, 84460J
 Mesinger, A., Aykutanalp, A., Vanzella, E., et al. 2015, *MNRAS*, 446, 566
 Oesch, P. A., van Dokkum, P. G., Illingworth, G. D., et al. 2015, *ApJ*, 804, L30
 Oke, J. B., & Gunn, J. E. 1983, *ApJ*, 266, 713
 Ono, Y., Ouchi, M., Mobasher, B., et al. 2012, *ApJ*, 744, 83
 Pentericci, L., Fontana, A., Vanzella, E., et al. 2011, *ApJ*, 743, 132
 Pentericci, L., Vanzella, E., Fontana, A., et al. 2014, *ApJ*, 793, 113
 Pradhan, A. K., Montenegro, M., Nahar, S. N., & Eissner, W. 2006, *MNRAS*, 366, L6
 Roberts-Borsani, G. W., Bouwens, R. J., Oesch, P. A., et al. 2015, *arXiv:1506.00854*
 Salpeter, E. E. 1955, *ApJ*, 121, 161
 Schenker, M. A., Ellis, R. S., Konidaris, N. P., & Stark, D. P. 2014, *ApJ*, 795, 20
 Schenker, M. A., Stark, D. P., Ellis, R. S., et al. 2012, *ApJ*, 744, 179
 Shibuya, T., Kashikawa, N., Ota, K., et al. 2012, *ApJ*, 752, 114
 Song, M., Finkelstein, S. L., Ashby, M. L. N., et al. 2015, *ApJ*, submitted (*arXiv:1507.05636*)
 Song, M., Finkelstein, S. L., Gebhardt, K., et al. 2014, *ApJ*, 791, 3
 Stark, D. P., Ellis, R. S., Chiu, K., Ouchi, M., & Bunker, A. 2010, *MNRAS*, 408, 1628
 Stark, D. P., Ellis, R. S., & Ouchi, M. 2011, *ApJ*, 728, L2
 Steidel, C. C., Erb, D. K., Shapley, A. E., et al. 2010, *ApJ*, 717, 289
 Tilvi, V., Papovich, C., Finkelstein, S. L., et al. 2014, *ApJ*, 794, 5
 Treu, T., Schmidt, K. B., Trenti, M., Bradley, L. D., & Stiavelli, M. 2013, *ApJ*, 775, L29
 Treu, T., Trenti, M., Stiavelli, M., Auger, M. W., & Bradley, L. D. 2012, *ApJ*, 747, 27
 Vanzella, E., de Barros, S., Vasei, K., et al. 2016, *arXiv:1602.00688*
 Vanzella, E., Pentericci, L., Fontana, A., et al. 2011, *ApJ*, 730, L35
 Wirth, G. D., Trump, J. R., Barro, G., et al. 2015, *AJ*, 150, 153
 Zitrin, A., Labbé, I., Belli, S., et al. 2015, *ApJ*, 810, L12